Artificial Compressibility Method and Lattice Boltzmann Method: Similarities and Differences

Artificial Compressibility Method and Lattice Boltzmann Method: Similarities and Differences

Taku Ohwada

Department of Aeronautics and Astronautics, Graduate School of Engineering, Kyoto University, Kyoto 606-8501, Japan

Pietro Asinari

Dipartimento di Energetica, Politecnico di Torino, Torino 10129, Italy

Daisuke Yabusaki

Department of Aeronautics and Astronautics, Graduate School of Engineering, Kyoto University, Kyoto 606-8501, Japan

Abstract

Both the artificial compressibility method and the lattice Boltzmann method yield the solutions of the incompressible Navier-Stokes equations in the limit of the vanishing Mach number. The inclusion of the bulk viscosity is one of the reasons for the success of the lattice Boltzmann method since it removes quickly the acoustic mode, which inevitably appears as the compressible effect, and contributes to the reinforcement of the stability. In the present paper, the robustness of the artificial compressibility method is enhanced by introducing a new dissipation term, which makes high cell-Reynolds number computation possible. The increase of the stability is also confirmed in the linear stability analysis; the magnitude of the eigenvalues for high wave numbers and low resolution are drastically reduced. Comparisons are made with the lattice Boltzmann method. It is confirmed that the fortified ACM is more robust as well as more accurate than the lattice Boltzmann method.

Key words: Incompressible Navier-Stokes Equations, Artificial Compressibility Method, Acoustic Wave, Lattice Boltzmann

1. INTRODUCTION

The similarities between the lattice Boltzmann method (LBM) and the artificial compressibility method (ACM) [3] are sometimes mentioned in the literature. It is well-known that the Chapman-Enskog expansion of the LBM updating rule derives the equation system that ACM is based on, i.e. the artificial compressibility equations (ACE), which consist of the same momentum equation as that of the incompressible Navier-Stokes equations (INSE) and an

artificial continuity equation with the pressure time derivative. ACE are also revived by summing up the equation systems derived by the more systematic expansion, i.e. the Hilbert expansion under the diffusive scaling. The lattice kinetic scheme (LKS), which is a variant of LBM, also emphasizes the similarity at the level of the computer programming despite the fact that LBM deals with the distribution function of gas molecules and ACM deals with only macroscopic variables. For a special value of the relaxation parameter in the LBM updating rule, an updated value of the distribution function is given only by that of the previous equilibrium function at a mesh point in the stencil, i.e. $f(t = n + 1, x_i, c_i) = f_e(t = n, x_i - c_i, c_i)$. Since the value of the equilibrium function f_e is characterized only by those of the macroscopic variables, i.e. $f_e(t, x_i, c_i) = \tilde{f}_e(h(t, x_i), c_i)$, where h stands for the macroscopic variables, the LKS updating rule is immediately recognized as a kind of purely macroscopic finite difference scheme. Indeed, by taking the moments of the LKS updating rule, we have a variant of ACM. Incidentally, a compact LKS with tunable viscosity is proposed on the basis of this recognition in Ref. [1].

The following points have been clarified by recent studies on LBM and ACM (Refs. [1, 10, 7]):

i) The applicability of LBM using usual compact stencils, such as D2Q9 and D3Q15, is validated only up to the Navier-Stokes level. The classic high order stress beyond Navier-Stokes, i.e. Burnett, super Burnett, etc., requires more discrete velocities.

ii) ACM is, in principle, tunable for Mach number even for the fixed resolution with respect to space and time. This property enables a drastic error reduction, i.e. the achievement of the fourth order accuracy in space and the second order accuracy in time.

In the present paper, we take the item i) for granted and treat LBM employing a usual compact stencil as one of INSE solvers. The item ii) does not mean the superiority of ACM over LBM immediately, since the performance of numerical methods is not evaluated only by the accuracy and the efficiency. It is said that LBM, in particular MRT-LBM [5, 6], has sufficient robustness, which is one of the reasons why LBM is successfully employed in various complex fluid flow simulations. In Sec. 2, we shall propose a simple method for enhancing the stability of ACM. The robustness of the fortified ACM will be examined numerically in Sec. 3 together with the Galilean invariance and the isotropy, which are also regarded as the important properties of fluid-dynamic solvers. LBM and ACM yield the INSE solutions in the limit of the vanishing Mach number and therefore the compressibility effect inevitably appears as the error. The compressibility error is categorized into the two modes, the acoustic mode, which is rapidly varying with respect to time, and the diffusive mode, which is slowly varying with respect to time. One of the main superiority of MRT-LBM over LBGK [8] lies in the capability of tuning the bulk viscosity. Owing to the sufficient bulk viscosity, MRT-LBM is capable of killing the acoustic mode quickly irrespective of the Reynolds number. The ACM proposed in Ref. [7]

is equipped with a different artificial dissipation mechanism for the suppression of the acoustic mode. A comparison between these different dissipation mechanisms will also be made in Sec. 3.

The drastic error reduction of ACM is brought by a Richardson extrapolation in the Mach number; the leading error of the diffusive mode is eliminated by taking a suitable linear combination of two ACM solutions for different values of the Mach number under the same resolution [7]. In the conventional LBM the Mach number is fixed for the fixed values of the mesh spacing and the time step. By changing the equation of state, however, it is possible to redesign LBM as the one with tunable Mach number [2, 11]. Sec. 4 is devoted to the discussion on this issue.

2. THEORY OF ACM

2.1. Basic equations

Our target equation system is the time-dependent INSE:

$$\frac{\partial u_i}{\partial x_i} = 0, \tag{1}$$

$$\frac{\partial u_i}{\partial t} + u_j \frac{\partial u_i}{\partial x_j} + \frac{\partial P}{\partial x_i} = \nu \frac{\partial^2 u_i}{\partial x_j^2} + f_i, \tag{2}$$

where x_i, t, u_i, P and f_i are dimensionless variables corresponding to the space coordinates, time, the flow velocity, the (kinematic) pressure, and the external force, respectively, and ν is the dimensionless kinematic viscosity, which is equal to the inverse Reynolds number, i.e. $\nu = 1/\mathrm{Re}$. In the original ACM, the solenoidal condition (1) is replaced by the artificial continuity equation:

$$k \frac{\partial P}{\partial t} + \frac{\partial u_i}{\partial x_i} = 0, \tag{3}$$

where k is a positive constant and its value is usually chosen from the range $0.1 \leq k \leq 10$. Equations (2) and (3) constitute ACE. In Ref. [7], the following modified artificial continuity equation is proposed:

$$\beta \epsilon^2 \Big(\frac{\partial P}{\partial t} + \gamma P \Big) + \frac{\partial u_i}{\partial x_i} = 0, \tag{4}$$

where γ is a positive function of t (it is treated as a constant in the present paper for simplicity), ϵ is a positive and small constant, i.e. $0 < \epsilon \ll 1$, and β is a positive constant of the order of unity. The term γP is for the suppression of the acoustic mode.

2.2. Diffusive mode and acoustic mode

Consider a slowly varying solution of ACE (2) and (4), i.e. $\partial_\alpha h = O(h)$ ($\alpha = t, x_i$, $h = u_i, P$). We expand the solution into the power series of ϵ^2:

$$h = h_{S0} + \epsilon^2 h_{S1} + \epsilon^4 h_{S2} + \cdots . \tag{5}$$

Substituting the solution in the above form into Eqs. (2) and (4) and equating the terms of the same order of power of ϵ^2, we get the PDE systems for the coefficient functions h_{Sm} ($m = 0, 1, 2, \cdots$):

$$\frac{\partial u_{iSm}}{\partial x_i} = -\beta\Big(\frac{\partial P_{Sm-1}}{\partial t} + \gamma P_{Sm-1}\Big), \tag{6}$$

$$\frac{\partial u_{iSm}}{\partial t} + \sum_{\substack{0\le a\le m\\ 0\le b\le m\\ a+b=m}} u_{jSa}\frac{u_{iSb}}{\partial x_j} + \frac{\partial P_{Sm}}{\partial x_i} = \nu\frac{\partial^2 u_{iSm}}{\partial x_k^2}, \tag{7}$$

where $P_{Sm-1} = 0$ for $m = 0$. The equation system for $m = 0$ is INSE and inhomogeneous Oseen-type equation systems follow from $m = 1$. There is only one inhomogeneous term in the equation system for $m = 1$. It appears in Eq. (6) and it is proportional to β, which implies that the leading error of the diffusive mode is linear in β. Thus, we can, in principle, cancel the leading error of $O(\epsilon^2)$ by combining two ACE solutions for different values of β. However, the above scenario does not take account of the acoustic mode, which inevitably appears in the computation of ACE if casual initial data, such as those for INSE, are employed. As previously mentioned, the term γP in Eq. (4) is to kill the acoustic mode. In order to illustrate the role of this term, we consider the linearized ACE for the acoustic scaling $(\tilde{t}, q, w_i) = (t/\epsilon, P/\epsilon, u_i/\epsilon^2)$. We refer the reader to Ref. [7] for the derivation of this scaling. The ACE linearized around a uniform state at rest are given by

$$\beta\Big(\frac{\partial q}{\partial \tilde{t}} + \gamma\epsilon q\Big) + \frac{\partial w_j}{\partial x_j} = 0, \tag{8}$$

$$\frac{\partial w_i}{\partial \tilde{t}} + \frac{\partial q}{\partial x_i} = \epsilon\nu\frac{\partial^2 w_i}{\partial x_j^2} \tag{9}$$

where the external force is omitted for simplicity. From the above equation system, we obtain the dissipative wave equation for P:

$$\frac{\partial^2 q}{\partial \tilde{t}^2} = (\frac{1}{\beta} + \epsilon^2\gamma\nu)\frac{\partial^2 q}{\partial x_j^2} - \epsilon\gamma\frac{\partial q}{\partial \tilde{t}} + \epsilon\nu\frac{\partial^3 q}{\partial x_j^2\partial \tilde{t}}. \tag{10}$$

The term γP in Eq. (4) acts like a viscous damper and it works uniformly for any wave number, while the dissipation due to the viscous term is proportional to the wave number squared.

2.3. Computation of ACM

In Ref. [7], the equation system (2) and (4) is cooked according to the following recipe.

i) As in the case of LBM, a structural mesh system with uniform mesh spacing is employed. The small parameter ϵ is employed as the mesh spacing. The time step Δt is $O(\epsilon^2)$.

ii) In the computation for obtaining the velocity and pressure fields at $t = \Delta t$ from those at $t = 0$, a two-step semi-implicit time-marching method is adopted. The flow velocity field at $t = \Delta t/2$ is computed first by the usual forward-Euler time-marching. Then, the pressure field at $t = \Delta t/2$ is computed by using the backward-Euler time-marching; the divergence of the velocity field at $t = \Delta t/2$ is employed in the computation. The second stage computes the velocity and pressure fields at $t = \Delta t$ by using the mid-point formula of numerical integration.

iii) For the suppression of the checkerboard instability, the artificial continuity equation employed in the second stage of the pressure update is modified as

$$\beta\epsilon^2\Big(\frac{\partial P}{\partial t} + \gamma P\Big) + \frac{\partial u_i}{\partial x_i} = \beta\mu\epsilon^3\Big(\frac{\partial^2 P}{\partial x_j^2} + \frac{\partial u_j}{\partial x_i}\frac{\partial u_i}{\partial x_j}\Big), \tag{11}$$

where μ is a positive constant of the order of unity.

iv) Each spatial derivative in the momentum equation is approximated by the corresponding central finite difference formula with fourth order accuracy (5 point formula). For each term on the right hand side of Eq. (11), the corresponding three point central finite formula suffices. The divergence of the flow velocity, which appears in the continuity equations (4) and (11), is computed with fourth order accuracy by using a compact stencil. For simplicity, let us consider the 2D case. Let p be one of the indices 1 and 2 and let q be the other index. The three point central finite difference approximation of $\partial u_p/\partial x_p$ (Einstein summation convention is not applied to it) yields the leading error $(\epsilon^2/6)\partial^3 u_p \partial x_p^3$. In the diffusive mode, the divergence of the flow velocity is $O(\epsilon^2)$, i.e. $\partial u_1/\partial x_1 + \partial u_2/\partial x_2 = O(\epsilon^2)$. Then, $\partial^3 u_p/\partial x_p^3 = -\partial^3 u_p/\partial x_p^2 \partial x_q + O(\epsilon^2)$. The mixed third order derivative can be computed with second order accuracy by using a 3×3 point stencil. Thus the divergence of the flow field is computed on a compact stencil with fourth order accuracy in the case of the diffusive mode.

v) For high order accurate treatment of the Dirichlet-type boundary condition, we refer the reader to Ref. [7], where the Numerov algorithm is locally applied to the mesh points next to boundaries.

We show the explicit finite difference formulas in the 2D case below. For ease of expression, we rewrite x_1, x_2, u_1, u_2, f_1, and f_2 as x, y, u, v, f_x, and

f_y, respectively.

$$u_{ij}^{n+1/2} = u_{ij}^n + \frac{\Delta t}{2}\Big(-u_{ij}^n D_x u_{ij}^n - v_{ij}^n D_y u_{ij}^n - D_x P_{ij}^n + \nu[D_{xx}+D_{yy}]u_{ij}^n + F_{ij}^n\Big), \quad (12)$$

$$v_{ij}^{n+1/2} = v_{ij}^n + \frac{\Delta t}{2}\Big(-u_{ij}^n D_x v_{ij}^n - v_{ij}^n D_y v_{ij}^n - D_y P_{ij}^n + \nu[D_{xx}+D_{yy}]v_{ij}^n + G_{ij}^n\Big), \quad (13)$$

$$P_{ij}^{n+1/2} = \Big(P_{ij}^n - \frac{\Delta t}{2\beta\epsilon^2}\mathcal{D}(u_{ij}^{n+1/2}, v_{ij}^{n+1/2})\Big)/(1+\frac{\gamma\Delta t}{2}), \quad (14)$$

$$\begin{aligned} u_{ij}^{n+1} = u_{ij}^n + \Delta t\Big(& - u_{ij}^{n+1/2} D_x u_{ij}^{n+1/2} - v_{ij}^{n+1/2} D_y u_{ij}^{n+1/2} \\ & - D_x P_{ij}^{n+1/2} + \nu[D_{xx}+D_{yy}]u_{ij}^{n+1/2} + F_{ij}^{n+1/2}\Big), \end{aligned} \quad (15)$$

$$\begin{aligned} v_{ij}^{n+1} = v_{ij}^n + \Delta t\Big(& - u_{ij}^{n+1/2} D_x v_{ij}^{n+1/2} - v_{ij}^{n+1/2} D_y v_{ij}^{n+1/2} \\ & - D_y P_{ij}^{n+1/2} + \nu[D_{xx}+D_{yy}]v_{ij}^{n+1/2} + G_{ij}^{n+1/2}\Big), \end{aligned} \quad (16)$$

$$\begin{aligned} P_{ij}^{n+1} = & P_{ij}^n + \Delta t\Big(- \gamma P_{ij}^{n+1/2} - \frac{1}{\beta\epsilon^2}\mathcal{D}(u_{ij}^{n+1/2}, v_{ij}^{n+1/2}) \\ & + \mu\epsilon[(\delta_{xx}+\delta_{yy})P_{ij}^{n+1/2} + 2(\delta_x v_{ij}^{n+1/2}\delta_y u_{ij}^{n+1/2} - \delta_x u_{ij}^{n+1/2}\delta_y v_{ij}^{n+1/2})]\Big), \end{aligned} \quad (17)$$

$$\mathcal{D}(u_{ij}^{n+1/2}, v_{ij}^{n+1/2}) = \delta_x u_{ij}^{n+1/2} + \delta_y v_{ij}^{n+1/2} + \frac{\epsilon^2}{6}(\delta_{xx}\delta_y v_{ij}^{n+1/2} + \delta_x \delta_{yy} u_{ij}^{n+1/2}), \quad (18)$$

where h_{ij}^α ($h = u, v, P$) is $h(\alpha\Delta t, x^{(i)}, y^{(j)})$; $x^{(i)} = i\epsilon$ and $y^{(j)} = j\epsilon$; $F_{ij}^\alpha = f_x(\alpha\Delta t, x^{(i)}, y^{(j)})$ and $G_{ij}^\alpha = f_y(\alpha\Delta t, x^{(i)}, y^{(j)})$; δ_x, δ_{xx}, δ_y, and δ_{yy} are three point central finite difference operators corresponding to ∂_x, ∂_{xx}, ∂_y, and ∂_{yy}, respectively; D_x, D_{xx}, D_y, and D_{yy} are five point central finite difference operators corresponding to ∂_x, ∂_{xx}, ∂_y, and ∂_{yy}, respectively.

2.4. Fortification of ACM

We consider a method for enhancing the stability of ACM. We add a high order dissipation term to the momentum equation:

$$\frac{\partial u_i}{\partial t} + u_j\frac{\partial u_i}{\partial x_j} + \frac{\partial P}{\partial x_i} = \nu\frac{\partial^2 u_i}{\partial x_j^2} + f_i - \epsilon^4\sum_{l\neq m} s_{lm}\frac{\partial^4 u_i}{\partial x_l^2 \partial x_m^2}, \quad (19)$$

where s_{lm} are constants of the order of unity. The term added to the momentum equation is $O(\epsilon^4)$ and the first two equation systems in the asymptotic analysis of the diffusive mode are not altered by this modification. We investigate the role of this term by carrying out the Von Neumann stability analysis using the ACE linearized around a uniform state at rest:

$$\beta\epsilon^2\Big(\frac{\partial P}{\partial t} + \gamma P\Big) + \Big(\frac{\partial u}{\partial x} + \frac{\partial v}{\partial y}\Big) = 0, \quad (20)$$

$$\left(\beta\epsilon^2\Big(\frac{\partial P}{\partial t}+\gamma P\Big)+\Big(\frac{\partial u}{\partial x}+\frac{\partial v}{\partial y}\Big)=\beta\mu\epsilon^3(\frac{\partial^2 P}{\partial x^2}+\frac{\partial^2 P}{\partial y^2})\right), \tag{21}$$

$$\frac{\partial u}{\partial t}+\frac{\partial P}{\partial x}=\nu\Big(\frac{\partial^2 u}{\partial x^2}+\frac{\partial^2 u}{\partial y^2}\Big)-s\epsilon^4\frac{\partial^4 u}{\partial x^2\partial y^2}, \tag{22}$$

$$\frac{\partial v}{\partial t}+\frac{\partial P}{\partial y}=\nu\Big(\frac{\partial^2 v}{\partial x^2}+\frac{\partial^2 v}{\partial y^2}\Big)-s\epsilon^4\frac{\partial^4 v}{\partial x^2\partial y^2}, \tag{23}$$

where $s = s_{12} = s_{21}$. The finite difference scheme for the above linearized equation system is made according to the recipe given in the previous subsection [Eq. (21) is employed in the second step of the time integration for P. See the recipe iii) in the previous subsection]. We assume the numerical solution in the form

$$\begin{pmatrix} u^n_{lm} \\ v^n_{lm} \\ P^n_{lm} \end{pmatrix} = \lambda^n \exp[\mathrm{i}\tilde{k}(l+m)] \begin{pmatrix} u^0 \\ v^0 \\ P^0 \end{pmatrix}, \tag{24}$$

where i is the imaginary number unit ($\mathrm{i}=\sqrt{-1}$) and $\tilde{k}$ is the normalized wave number ($\tilde{k}/\epsilon$ is the wave number). We consider the $(1,1)$ direction in the (x,y) plane as the direction of the travel of waves. The time step Δt is assumed to be $O(\epsilon^2)$ and it will be expressed as $\Delta t = \tau\epsilon^2$. The eigenvalue λ depends on ν, β, γ, μ, s, ϵ, τ, and $\tilde{k}$. The range of $\tilde{k}$ is $0 \le \tilde{k} \le \pi$ since the resolution for one wavelength requires at least two mesh points. In the case of the original ACM, i.e. $\gamma = \mu = s = 0$, we obtain the simple diffusive CFL condition $\nu\tau \le 3/16$, which is derived from the condition of the eigenvalue for the transverse mode (shear without pressure variation). The conditions for the other two eigenvalues, which correspond to the longitudinal mode, give the acoustic CFL condition, which is $\tau < 1.211566\beta^{1/2}$ for $\nu = 0$. Next we consider the general case of γ, ν, and s. Let λ_a and λ_b be the eigenvalues for the longitudinal mode and let λ_c be that for the transverse mode. The eigenvectors corresponding to λ_a and λ_b are expressed as $(P_a, 1, 1)^T$ and $(P_b, 1, 1)^T$, respectively, and that corresponding to λ_c is given by $(0, -1, 1)^T$, where P_a and P_b are complex valued functions of $(\nu, \beta, \gamma, \mu, s, \epsilon, \tau, \tilde{k})$. In the limit of $\tilde{k} \to \pi$, we have $|P_a| \to \infty$, $P_b \to 0$, and $\lambda_b - \lambda_c \to 0$. That is, the eigenvector for λ_a becomes $(1, 0, 0)^T$ and that for λ_b becomes $(0, 1, 1)^T$. Then, we can choose $(0, 1, 0)^T$ and $(0, 0, 1)^T$ as the normalized eigenvectors for the degenerate eigenvalue $\lambda_b (= \lambda_c)$. In this limit, the eigenvalue λ_a is given by

$$\lambda_a = \frac{2 - 16\epsilon\mu\tau - \epsilon^2\gamma\tau}{2 + \epsilon^2\gamma\tau}. \tag{25}$$

We have $\lambda_a = 1$ for $\gamma = \mu = 0$, which shows that the checkerboard instability for the pressure is not suppressed. The terms multiplied by these two positive constants contribute to the suppression of it; the term multiplied by γ is $O(\epsilon^2)$ and the one multiplied by μ is $O(\epsilon)$. The checkerboard instability can occur in an actual nonlinear computation for $\mu = 0$ (see Ref. [7]). The role of the term

multiplied by s is as follows. The limiting value of $\lambda_b(=\lambda_c)$ is expressed as the sum

$$\lambda_b(=\lambda_c) = \lambda_{b1} + \lambda_{b2}, \tag{26}$$

where

$$\lambda_{b1} = 1 - \frac{32\nu\tau}{3} + \frac{512\nu^2\tau^2}{9}, \tag{27}$$

$$\lambda_{b2} = 128\epsilon^4 s^2\tau^2 + 16\epsilon^2 s\tau(\frac{32\nu\tau}{3} - 1). \tag{28}$$

We notice $1/2 \leq \lambda_{b1} \leq 1$ for $0 \leq \nu\tau \leq 3/16$ (cf. the diffusive CFL condition for $\gamma = \mu = s = 0$). As $\nu\tau \to 0$ or $\nu\tau \to 3/16$, λ_{b1} approaches to 1. Therefore, for $s = 0$, $\lambda_b(=\lambda_c)$ is nearly equal to unity around these limiting values of $\nu\tau$, which is not preferable as in the case of λ_a. A positive value of s reduces the value of λ_b for $\nu\tau < 3/32$ and a negative value of s reduces it for $3/32 < \nu\tau$. The magnitudes of the eigenvalues $|\lambda|$ ($\lambda = \lambda_a, \lambda_b, \lambda_c$) vs. ϵ for ($\nu = 0.001$, $\beta = 2$, $\gamma = \mu = \tau = 1$) is shown in Fig. 1. It is seen that the magnitudes of λ_b and λ_c are remarkably reduced by changing the value of s from 0 to 2.

2.5. Bulk viscosity

The usefulness of the inclusion of the bulk viscosity for ACM was pointed out in Ref. [9] prior to the development of MRT-LBM [5]. In order to investigate the role of the bulk viscosity in ACM, we consider the following ACE.

$$\beta\epsilon^2\frac{\partial P}{\partial t} + \frac{\partial u_j}{\partial x_j} = 0, \tag{29}$$

$$\frac{\partial u_i}{\partial t} + u_j\frac{\partial u_i}{\partial x_j} + \frac{\partial P}{\partial x_i} = \nu\frac{\partial^2 u_i}{\partial x_j^2} + f_i + \chi\frac{\partial^2 u_j}{\partial x_i \partial x_j}. \tag{30}$$

Although χ does not correspond to the (kinematic) bulk viscosity in general, we simply call χ the bulk viscosity here. Incidentally, in the MRT-LBM for D2Q9 stencil [6], χ is given by $(1/s_2 - 1/2)/3$. We consider the linearized ACE for the acoustic scaling $(\tilde{t}, q, w_i) = (t/\epsilon, P/\epsilon, u_i/\epsilon^2)$:

$$\beta\frac{\partial q}{\partial \tilde{t}} + \frac{\partial w_j}{\partial x_j} = 0, \tag{31}$$

$$\frac{\partial w_i}{\partial \tilde{t}} + \frac{\partial q}{\partial x_i} = \epsilon\nu\frac{\partial^2 w_i}{\partial x_j^2} + \epsilon\chi\frac{\partial^2 w_j}{\partial x_i \partial x_j} \tag{32}$$

where the external force is omitted. From the above equation system, we obtain

$$\frac{\partial^2 q}{\partial \tilde{t}^2} = \frac{1}{\beta}\frac{\partial^2 q}{\partial x_k^2} + \epsilon(\nu + \chi)\frac{\partial^3 q}{\partial x_k^2 \partial \tilde{t}}. \tag{33}$$

We notice that both the viscosity and the bulk viscosity make the same contribution to the suppression of the acoustic mode. The contribution of the bulk viscosity to the diffusive mode appears as the leading error of $O(\epsilon^2)$. In fact, by

carrying out the similar asymptotic analysis for the diffusive mode of solution of Eqs. (29) and (30), we have the equation system for the leading error:

$$\frac{\partial u_{iS1}}{\partial x_i} = -\beta \frac{\partial P_{S0}}{\partial t}, \tag{34}$$

$$\frac{\partial u_{iS1}}{\partial t} + u_{jS0}\frac{u_{iS1}}{\partial x_j} + u_{jS1}\frac{u_{iS0}}{\partial x_j} + \frac{\partial P_{S1}}{\partial x_i} = \nu \frac{\partial^2 u_{iS1}}{\partial x_k^2} + \chi \frac{\partial^2 u_{jS1}}{\partial x_i \partial x_j}. \tag{35}$$

From Eq. (34) we notice

$$\chi \frac{\partial^3 u_{jS1}}{\partial x_i \partial x_j} = -\beta \chi \frac{\partial^2 P_{S0}}{\partial x_i \partial t}, \tag{36}$$

which shows that both of the two inhomogeneous terms in the above Oseen-type equation system are proportional to β. Therefore, the leading error of the diffusive mode can be eliminated in principle as before.

Finally, we mention the art of the approximation of the bulk viscosity term $\chi(\partial^2 u_j/\partial x_i \partial x_j)$ in the numerical computation. For the cancellation of the leading error of the diffusive mode, the accuracy of the approximation must be at least fourth order. Although the use of the five point central difference approximation of the second order derivatives, i.e. $\chi(D_{xx}u_{ij}^n + D_{xy}v_{ij}^n)$ and $\chi(D_{xy}u_{ij}^n + D_{yy}v_{ij}^n)$, seems to be reasonable, however, it does not work well; the fourth order convergence rate is not observed clearly in the numerical computation. This is considered to be due to the weak constraint on the linearity of the bulk viscosity term in β at the numerical level. In order to enhance the constraint, we apply the three point central finite difference operators to $\mathcal{D}(u_{ij}^n, v_{ij}^n)$, i.e. $\chi\delta_x\mathcal{D}(u_{ij}^n, v_{ij}^n)$ and $\chi\delta_y\mathcal{D}(u_{ij}^n, v_{ij}^n)$ [see Eq. (18)]. The employment of the second order accurate finite difference operators δ_x and δ_y is legitimated by the fact that the divergence of the flow velocity in the diffusive mode is $O(\epsilon^2)$ and the truncation errors of its first order derivatives are $O(\epsilon^4)$. Incidentally, the finite difference approximations of the divergence $\chi(D_{xx}u_{ij}^n + D_{xy}v_{ij}^n)$ and $\chi\delta_x\mathcal{D}(u_{ij}^n, v_{ij}^n)$ employ 5×5 stencils.

The linear stability analysis of the ACM for Eqs. (29) and (30) can be done in the same way as in the case of the fortified ACM for Eqs. (4) and (19). The cure for the checkerboard instability is also implemented in the same way. The structure of the eigenspace is similar to that of the previous case. We express the three eigenvalues in the same way as before. In the limit of $\tilde{k} = \pi$, λ_a is given by

$$\lambda_a = 1 - 8\epsilon\mu\tau, \tag{37}$$

which corresponds to Eq. (25) for $\gamma = 0$. As in the previous case, λ_b becomes equal to λ_c in this limit. $\lambda_b (= \lambda_c)$ is given by

$$\lambda_b = 1 - \frac{32\nu\tau}{3} + \frac{512\nu^2\tau^2}{9}, \tag{38}$$

which corresponds to $\lambda_{b2} = 0$ in the previous case. The bulk viscosity terms do not contribute to the reduction of the eigenvalues for $\tilde{k} = \pi$; they depend on

χ in the case where the bulk viscosity terms in the momentum equations are approximated as $\chi(D_{xx}u + D_{xy}v)$ and $\chi(D_{xy}u + D_{yy}v)$. This implies that the effect of the bulk viscosity depends on the structure of numerical scheme. The magnitudes of the eigenvalues $|\lambda|$ ($\lambda = \lambda_a, \lambda_b, \lambda_c$) versus ϵ for $\chi = (1/s_2 - 1/2)/3$ with $s_2 = 1.63$ ($\nu = 0.001$, $\beta = 2$, $\mu = \tau = 1$) are shown in Fig. 2; $s_2 = 1.63$ is adopted here according to Ref. [6]. It should be remarked that the eigenvalue of the transverse mode λ_c is independent of χ irrespective of the wave number.

3. ROBUSTNESS, GALILEAN INVARIANCE, AND ISOTROPY

As the test problems, we consider the generalized Taylor-Green problem and the lid-driven cavity flow problem in two space dimension.

3.1. Generalized Taylor-Green problem

The problem of Taylor-Green vortices is widely employed as the test case of various INSE solvers because of the availability of its simple analytical solution. In Ref. [7] this problem is generalized by introducing a forcing in order to make the solution periodic with respect to time as well. By adding the forcing

$$\begin{pmatrix} f_x \\ f_y \end{pmatrix} = (2k^2\nu\cos t - \sin t) \begin{pmatrix} \sin[k(x-u_0t)]\cos[k(y-v_0t)] \\ -\cos[k(x-u_0t)]\sin[k(y-v_0t)] \end{pmatrix}, \tag{39}$$

the following flow and pressure fields satisfy INSE.

$$\begin{aligned} u(x,y,t) &= u_0 + \sin[k(x-u_0t)]\cos[k(y-v_0t)]\cos t, \\ v(x,y,t) &= v_0 - \cos[k(x-u_0t)]\sin[k(y-v_0t)]\cos t, \\ P(x,y,t) &= \frac{1}{4}\{\cos[2k(x-u_0t)] + \cos[2k(y-v_0t)]\}\cos^2 t, \end{aligned} \tag{40}$$

where u_0, v_0, and k are constants. We study the case where the offset velocity (u_0, v_0) is expressed as $U(\cos\theta, \sin\theta)$. The initial data for the numerical computation of ACM (and LBM) is given by Eq. (40) with $t = 0$ and the periodic boundary condition is employed. Hereafter, the values of the parameters ν, γ, μ, τ, s, and s_2 will be $\nu = 0.001$, $\gamma = 1$, $\mu = 1$, $\tau = 1$, $s = 2$, and $s_2 = 1.63$, respectively, and the result of ACM will mean the one produced by the Richardson extrapolation from the results of the fortified ACM on the basis of Eqs. (4) and (19) for $\beta = 2, 4$ under the same resolution ϵ, unless otherwise stated. The ACM for Eqs. (29) and (30) [$\chi = (1/s_2 - 1/2)/3$] will be called ACM-Bulk and its results will be computed by the Richardson extrapolation from those for $\beta = 2, 4$.

The time histories of L^1 error $\tilde{E}[h]$ ($h = u, P$) of the ACM result in the case of $(k, U, \theta, \epsilon) = (1, 1, \pi/12, \pi/32)$ are shown in Fig. 3. For comparison, the results of LBGK [8], MRT-LBM [6, 4], and ACM-Bulk are shown in the figure. While LBGK exhibits the acoustic mode significantly even around t=100, the quick suppression of the acoustic mode is confirmed for the other methods; while $\chi = \nu = 0.001$ for LBGK, $\chi = 0.0378$ ($s_2 = 1.63$) for MRT-LBM and ACM-Bulk. As mentioned previously, the viscous dissipation for the acoustic mode

increases when the wave number increases. For $k = 4$, the acoustic mode is suppressed sufficiently at $t = 100$ even in the case of LBGK. The convergence rates for $k = 4$ are shown in Fig.4, where the results of ACM and ACM-Bulk are shown together with those for LBGK and MRT-LBM. While LBGK and MRT-LBM exhibit the second order convergence rate, both of the ACMs exhibit nearly fourth order convergence rate. ACM-Bulk yields better results than the fortified ACM with the additional dissipation term of $O(\epsilon^4)$.

As the test of Galilean invariance, we carried out the computation for $k = 1$ and various values of U and θ. The L^∞ errors of ACM at $t = 100$ for $\theta = \pi/12$, $U = 0, 1$ are shown in Fig. 5 and those for $U = 1$ and $\theta = 0, \pi/12, \pi/6, \pi/4$ are shown in Fig. 6. In these figures, the results of MRT-LBM are also shown for comparison. While INSE is invariant under the Galilean transformation, ACE is not. Thus the difference in the offset velocity (u_0, v_0) appears as that of the error. The principal part of the error of ACM is eliminated by the Richardson extrapolation and ACM yields better results than MRT-LBM.

Concerning the isotropy, we carried out the computations for $(k, U, \theta) = (1, 1, 0)$ in the domain $(0 \le X \le 2\sqrt{2}\pi) \times (0 \le Y \le 2\sqrt{2}\pi)$, where $X = (x + y)/\sqrt{2}$ and $Y = (-x + y)/\sqrt{2}$, using uniform mesh systems for X and Y. The periodic boundary condition can still be employed in this case. The computation for the XY coordinate system corresponds to 45 degree clockwise rotation of the solution (40) around the origin. The results of ACM are shown in Fig. 7 together with those of MRT-LBM. Although any special care is not devoted to the isotropy in the case of ACM (the diagonal points in the stencil are not employed in the approximation of the spatial derivatives in the momentum equation), it yields better results than MRT-LBM. The present test is only for 45 degree rotation and is not sufficient. The tests for other angles are interesting but they could not be done because of the unavailability of the periodic boundary condition.

3.2. Lid-driven cavity flow

As the second test problem, we consider the standard lid-driven cavity flow problem, i.e. the fluid motion in a square domain $\Omega = [0 \le x \le 1] \times [0 \le y \le 1]$ consisting of the top side ($y = 1$) with the imposed velocity ($u = 1$ and $v = 0$) and the other three sides at rest. As the initial data, the impulse start from the homogeneous state $u = v = P = 0$ was employed. Because of the discontinuities with respect to space and time, the regularity of solution is obviously lost. The computation of ACM and LBM were carried out for $\nu = 0.0002$ under the condition $\sqrt{\beta}\epsilon = 0.3$, which corresponds to the case where the Mach number based on the speed of the moving wall is 0.3, and $\Delta t = 0.24\epsilon$. The relax of the acoustic CFL condition is usually done for fast convergence to the steady state. Consequently, the time step is proportional to the mesh spacing but τ is inversely proportional to the mesh spacing, i.e. $\tau = 0.24/\epsilon$. According to the diffusive CFL condition for $\gamma = \mu = s = 0$, $\nu\tau \le 3/16$, the stability region is $1/3906 \lesssim \epsilon$. Therefore this strategy should be legitimated if an effectively exact solution is obtained before the breakdown of the computation; an accurate result is obtained for $\epsilon = 1/256$ ($\gamma = 0$, $\mu = 1$, and $s = 0$) in Ref. [7]. The reason

why we revisit the problem in this paper is to demonstrate the robustness of the fortified ACM for low resolution regime, i.e. high cell-Reynolds number.

In the case of $s = 0$ ($\gamma = 0$ and $\mu = 1$), the computation is unstable for $\epsilon = 1/64$ and it becomes stable up to the establishment of the steady state for $\epsilon = 1/96$. In the case of $s = 2$ ($\gamma = 0$, and $\mu = 1$), the computation is stable even for $\epsilon = 1/32$; the cell-Reynolds number is 156.25. According to the linear stability analysis (Sec. 2.4), the stability is enhanced by changing the value of s from 0 to 2 (Fig. 1). The increase of the stability by the new artificial dissipation term $-s\partial_{xx}\partial_{yy}u_i$ is also confirmed in the present case (no figure); β and τ are function of ϵ in the above strategy of fast convergence to the steady state. In the case of ACM-Bulk, however, the increase of the stability is not confirmed; it sometimes spoils the stability. On the other hand, the computation of MRT-LBM ($s_2 = 1.63$, $\chi \sim 0.0378$) is stable for $\epsilon = 1/96$ but is not for $\epsilon = 1/64$. In the case of $s_2 = 1$, i.e. $\chi \sim 0.1667$, the computation is stable for $\epsilon = 1/64$ but it is not for $\epsilon = 1/32$, which shows that the increase of the bulk viscosity enhances the stability in the case of MRT-LBM. Incidentally, the computation of LBGK ($\chi = 0.0002$) is still unstable even for $\epsilon = 1/128$.

4. EXTRAPOLATION IN THE MACH NUMBER FOR LBM

In the ACM, tuning the Mach number for the fixed resolution with respect to space and time (and consequently combining different solutions) is the key to achieve a drastic error reduction and to gain two orders of accuracy. Actually it is possible to follow the same recipe in LBM by changing the equation of state [2, 11]. The explanation of the theory will be for LBGK for simplicity but the exhibition of the numerical results will be for MRT-LBM. The dimensionless form of the discrete velocity model of the simplified BGK equation is written as

$$\frac{\partial F}{\partial \hat{t}} + V_i \frac{\partial F}{\partial \hat{x}_i} = \lambda \left(F_e - F \right), \tag{41}$$

where V_i is the dimensionless molecular velocity on the lattice, i.e. V_i belongs to a set of Q permitted velocities, F and F_e are lists with Q elements and their elements are functions of $\hat{t}$ and $\hat{x}_i$. In the above dimensionless equation, the time, space coordinate, and molecular velocity are nondimensionalized as described for the original physical model. Moreover λ, which will be employed as a tuning parameter of LBM, is regarded as a constant of the order of unity. In D2Q9 model, the molecular velocity V_i has the following 9 values:

$$V_1 = \left[\begin{array}{ccccccccc} 0 & 1 & 0 & -1 & 0 & 1 & -1 & -1 & 1 \end{array} \right]^T, \tag{42}$$

$$V_2 = \left[\begin{array}{ccccccccc} 0 & 0 & 1 & 0 & -1 & 1 & 1 & -1 & -1 \end{array} \right]^T. \tag{43}$$

Consequently the components of the molecular velocity V_1, V_2, the discrete distribution function F and the discrete equilibrium distribution F_e are all lists

with 9 elements. Unlike what is usually done, we define the equilibrium F_e by

$$F_e = \begin{bmatrix} (9-5\varphi)/9\,\hat{\rho} - 2/3\,\hat{u}_1^2 - 2/3\,\hat{u}_2^2, \\ \varphi/9\,\hat{\rho} + 1/3\,\hat{u}_1 + 1/3\,\hat{u}_1^2 - 1/6\,\hat{u}_2^2, \\ \varphi/9\,\hat{\rho} + 1/3\,\hat{u}_2 + 1/3\,\hat{u}_2^2 - 1/6\,\hat{u}_1^2, \\ \varphi/9\,\hat{\rho} - 1/3\,\hat{u}_1 + 1/3\,\hat{u}_1^2 - 1/6\,\hat{u}_2^2, \\ \varphi/9\,\hat{\rho} - 1/3\,\hat{u}_2 + 1/3\,\hat{u}_2^2 - 1/6\,\hat{u}_1^2, \\ \varphi/36\,\hat{\rho} + 1/12\,(\hat{u}_1+\hat{u}_2) + 1/8\,(\hat{u}_1+\hat{u}_2)^2 - 1/24\,(\hat{u}_1^2+\hat{u}_2^2), \\ \varphi/36\,\hat{\rho} - 1/12\,(\hat{u}_1-\hat{u}_2) + 1/8\,(-\hat{u}_1+\hat{u}_2)^2 - 1/24\,(\hat{u}_1^2+\hat{u}_2^2), \\ \varphi/36\,\hat{\rho} - 1/12\,(\hat{u}_1+\hat{u}_2) + 1/8\,(-\hat{u}_1-\hat{u}_2)^2 - 1/24\,(\hat{u}_1^2+\hat{u}_2^2), \\ \varphi/36\,\hat{\rho} + 1/12\,(\hat{u}_1-\hat{u}_2) + 1/8\,(\hat{u}_1-\hat{u}_2)^2 - 1/24\,(\hat{u}_1^2+\hat{u}_2^2) \end{bmatrix}, \quad (44)$$

where $\hat{p} = \varphi\hat{\rho}/3$ and φ is a tunable parameter (for stability reasons $\varphi \leq 1$). $\hat{\rho}$, $\hat{u}_1$ and $\hat{u}_2$ are obtained as the moments of F:

$$\hat{\rho} = \langle F \rangle, \qquad \hat{u}_i = \langle V_i F \rangle. \quad (45)$$

In case $\varphi = 1$, the usual equilibrium is recovered. Recalling the discussion reported in Ref. [6], the previous equilibrium corresponds to set $c_1 = -2$, $\alpha_2 = 8\varphi - 16$, $\alpha_3 = -12\varphi + 16$, $\gamma_1 = 2/3$, $\gamma_2 = 18$, $\gamma_3 = 2/3$ and $\gamma_4 = 18$. The previous choice corresponds to the optimal stability strategy suggested in Ref. [6] and found by means of linear stability analysis, with the exception of parameter α_2, which was suggested to be $\alpha_2 = -8$. The optimal value is recovered in case $\varphi = 1$, but it cannot be fixed in general, if one wants to generalize the equation of state as in the present case.

LBM computation is nothing more than the forward Euler time integration formula of Eq. (41) with the time step of the unity:

$$F(\hat{t}+1, \hat{x}_i, V_i) = F(\hat{t}, \hat{x}_i - V_i, V_i) + \lambda\, G(\hat{t}, \hat{x}_i - V_i, V_i), \quad (46)$$

where

$$G = F_e - F. \quad (47)$$

Recall that the unit of space coordinate and that of time variable in Eq. (46) are the mean free path $l_c (= cT_c)$ and the mean collision time T_c, respectively. They are not appropriate as the characteristic scales for flow field in the continuum limit. Introducing a proper scaling in Eq.(46), i.e. assuming $\hat{t} = t/\epsilon^2$ and $\hat{x}_i = x_i/\epsilon$, yields

$$F(t+\epsilon^2, x_i, V_i) = F(t, x_i - V_i\epsilon, V_i) + \lambda\, G(t, x_i - V_i\epsilon, V_i). \quad (48)$$

We express $F(t+\epsilon^2, x_i, V_i)$, $F(t, x_i - V_i\epsilon, V_i)$, and $G(t, x_i - V_i\epsilon, V_i)$ as their Taylor expansions around (t, x_i). Next we assume F in the form

$$F = F^* + \epsilon F^{(1)} + \epsilon^2 F^{(2)} + \cdots, \quad (49)$$

and $\hat{\rho}$ and $\hat{u}_i$ are also expanded:

$$\hat{\rho} = 1 + \epsilon\rho^{(1)} + \epsilon^2\rho^{(2)} + \cdots, \quad (50)$$

$$\hat{u}_i = \epsilon u_i^{(1)} + \epsilon^2 u_i^{(2)} + \cdots , \tag{51}$$

Corresponding to the expansion, F_e is expressed in the form:

$$F_e = F^* + \epsilon F_e^{(1)} + \epsilon^2 F_e^{(2)} + \cdots , \tag{52}$$

$$G = \epsilon G^{(1)} + \epsilon^2 G^{(2)} + \cdots , \tag{53}$$

where

$$G^{(k)} = F_e^{(k)} - F^{(k)}. \tag{54}$$

Substituting the above expansions into Eq. (48) and equating the terms of the same order of power of ϵ, we derive the expressions for the distribution function coefficients $F^{(k)}$ $(k = 1, 2, \cdots)$. From the orthogonality conditions $\langle G^{(m)} \rangle = 0$ and $\langle V_k G^{(m)} \rangle = 0$, we have the PDE systems for $p^{(m)} = \varphi \rho^{(m)}/3$ and $u_i^{(m)}$. It is possible to prove that the leading pressure field is uniform, i.e. $p^{(1)} = p^{(1)}(t)$, and in various situations, such as the problem in a closed domain, where the total mass in the domain is constant, we can naturally assume $p^{(1)} = 0$. The coefficients $p^{(2)}$ and $u_i^{(1)}$ satisfy the incompressible Navier-Stokes system of equations. The coefficients $p^{(3)}$ and $u_i^{(2)}$ constitute the homogeneous Oseen system and its solution from homogeneous initial data and boundary condition is zero. Hence the leading errors of the numerical scheme are ruled by the coefficients $p^{(4)}$ and $u_i^{(3)}$, namely

$$\beta \frac{\partial p^{(2)}}{\partial t} + \frac{\partial u_i^{(3)}}{\partial x_i} = 0, \tag{55}$$

$$\frac{\partial u_i^{(3)}}{\partial t} + \frac{\partial}{\partial x_j}(u_i^{(1)} u_j^{(3)} + u_i^{(3)} u_j^{(1)}) + \frac{\partial p^{(4)}}{\partial x_i} = \frac{\omega_1}{3} \frac{\partial^2 u_i^{(3)}}{\partial x_k^2} + \omega_1 \left(1 - \frac{2}{3}\beta\right) \frac{\partial^2 p^{(2)}}{\partial x_i \partial t} + I_3, \tag{56}$$

where $\beta = 3/\varphi$ and the inhomogeneous term I_3 consists of the lower moments and its derivatives (see Appendix B of Ref. [1] for the exact expression of I_3). Clearly looking at the last driving forces in Eq. (56), it is possible to distinguish two contributions, both driven by the solution of the incompressible Navier-Stokes: the first is independent of β, while the second is linearly dependent on β. Hence it is possible to define also for LBM a Richardson extrapolation in the Mach number. Essentially an improved solution of LBM, getting rid of the error part linearly depending on β, is obtained as a suitable linear combination of two solutions for different $\beta(\varphi)$ under the same resolution, although no improvement in the order of accuracy of the method is expected.

The MRT-LBM computations of the generalized Taylor-Green problem of $(k, U, \theta) = (1, 1, \pi/12)$ were carried out for $\varphi = 1$ and $\varphi = 1/2$, which correspond to $\beta = 3$ and $\beta = 6$, respectively. The results are shown in Fig. 8 together with the results of the fortified ACM (Richardson extrapolation for $\beta = 3, 6$, $s = 2$). By the Richardson extrapolation, the error of LBM is considerably reduced, although the convergence rate is still second order as predicted theoretically.

5. Concluding Remarks

LBM can be regarded as a sort of microscopic ACM in the sense that it deals with the distribution function of gas molecules and its asymptotic expansion derives ACE. While the classic ACM can achieve high order accuracy by the Richardson extrapolation technique, the truncation error and the intrinsic high order (fake on usual compact stencils) stress prevent the complete removal of the leading error of the diffusive mode of the microscopic ACM. By careful tune on the basis of the linear stability analysis, MRT-LBM acquires the fine properties for the Galilean invariance and the isotropy. In the present study, the linear stability analysis was employed only for the confirmation of the robustness of ACM and any special care was not devoted to the improvement of the Galilean invariance and the isotropy. Fortunately, the Richardson extrapolation compensates for the lack of the effort and it enables ACM to yield better results than that of LBM at least in the generalized Taylor-Green problem. The fourth order accuracy isn space (the second order accuracy in time) is also confirmed in the ACM computation with the bulk viscosity. However, the bulk viscosity spoils the stability in some cases of lid-driven cavity flow problem, which is in contrast to the case of MRT-LBM. Since the classic ACM deals with only macroscopic variables, its improvement seems to be more feasible than that of LBM. ACM was developed about 40 years ago. The present study shows that ACM is still worth while being in the limelight.

Acknowledgements

The present study is supported from Japan Society for the Promotion of Science (JSPS) under Grant-in-Aid for Scientific Research (C) No.21560173.

References

[1] P. Asinari and T. Ohwada, "Connection between kinetic methods for fluid-dynamic equations and macroscopic finite-difference schemes", Comput. Math. Appl. **58**, 841–861 (2009).

[2] H. Chen, S. Chen, and W.H. Matthaeus, "Recovery of the Navier-Stokes equations using a lattice-gas Boltzmann method", Phys. Rev. A **45**, R5339 – R5342 (1992).

[3] A. J. Chorin, "A numerical method for solving incompressible viscous flow problems," J. Comput. Phys. **2**, 12–26 (1967).

[4] Z. Guo, C. Zheng, and B. Shi, "Lattice Boltzmann equation with multiple effective relaxation times for gaseous microscale flow," Phys. Rev. E **77**, 036707 (2008).

[5] D. d'Humières, "Generalized lattice Boltzmann equations", In *Rarefied gas dynamics: theory and simulations*, B.D. Shizgal and D.P. Weaver (Eds.), *Prog. Astronaut. Aeronaut.*, 159:450, 1992.

[6] P. Lallemand, and L.-S. Luo, "Theory of the lattice Boltzmann method: Dispersion, dissipation, isotropy, Galilean invariance, and stability", *Phys. Rev. E*, 61:6546 (2000).

[7] T. Ohwada and P. Asinari, "Artificial compressibility method revisited: Asymptotic numerical method for incompressible Navier-Stokes equations", J. Comput. Phys. (submitted).

[8] Y. Qian, D. d'Humières, and P. Lallemand, "Lattice BGK models for Navier-Stokes equation", Europhys. Lett. **17** 479–484 (1992).

[9] J.D. Ramshaw and V.A. Mousseau, "Accelerated artificial compressibility method for steady-state incompressibility flow calculations," Comput. & Fluids **18** 361–367 (1990).

[10] R. Rubinstein and L.-S. Luo, "Theory of Lattice Boltzmann equation: Symmetry properties of discrete velocity sets", *Phys. Rev. E*, 77:036709 (2008).

[11] X. Shan, G.D. Doolen, "Multicomponent lattice Boltzmann model with interparticle interaction", J. Stat. Phys. **81**, 379-393 (1995).

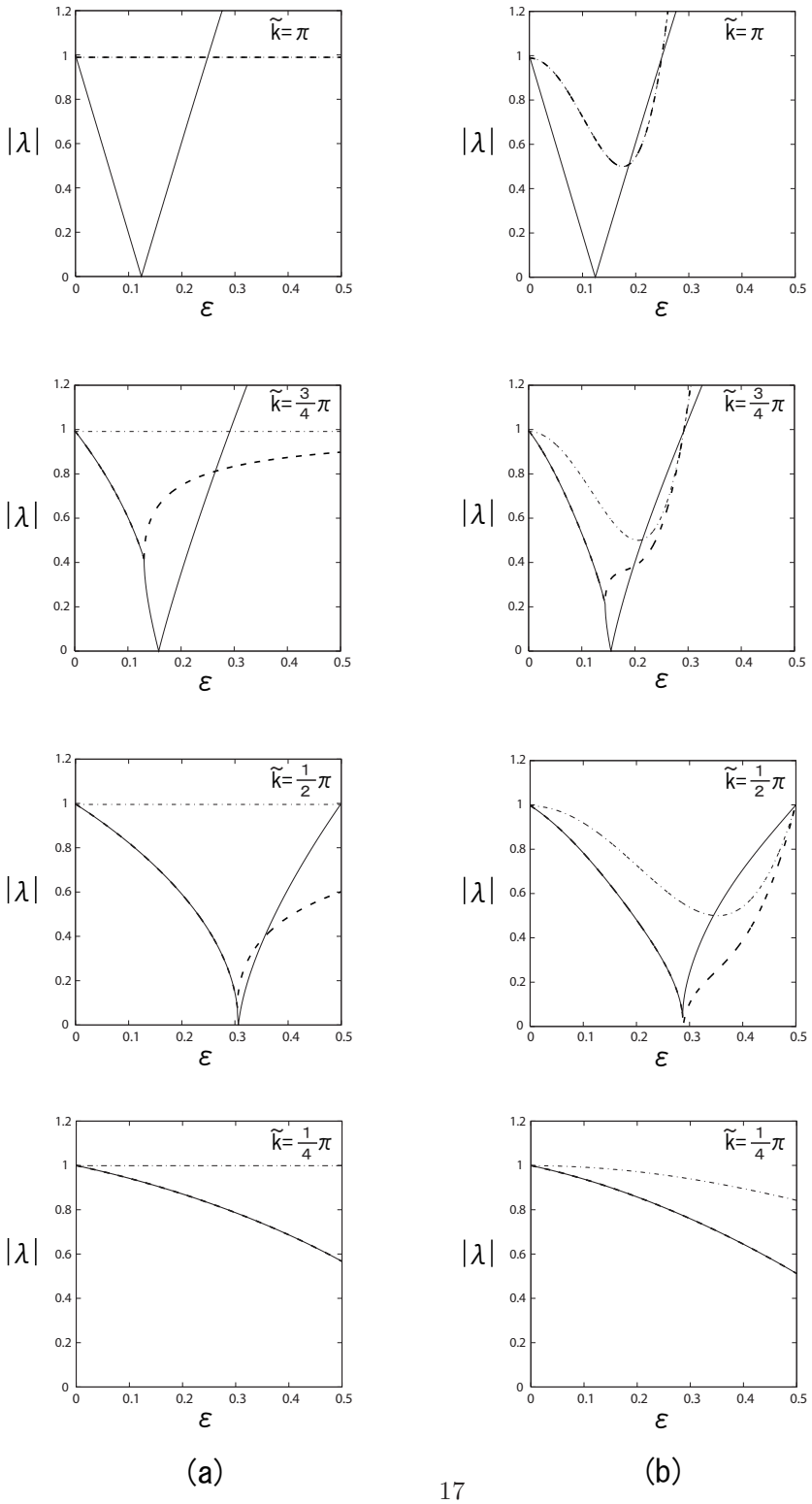

Figure 1: The magnitude of the eigenvalues for ACM versus ϵ. (a) $s = 0$ and (b) $s = 2$. The other parameters are $\nu = 0.001$, $\beta = 2$, $\gamma = 1$, $\mu = 1$, and $\tau = 1$ and they are common for (a) and (b). The solid line, the dashed line, and the dash dotted line indicate $|\lambda_a|$, $|\lambda_b|$, and $|\lambda_c|$, respectively.

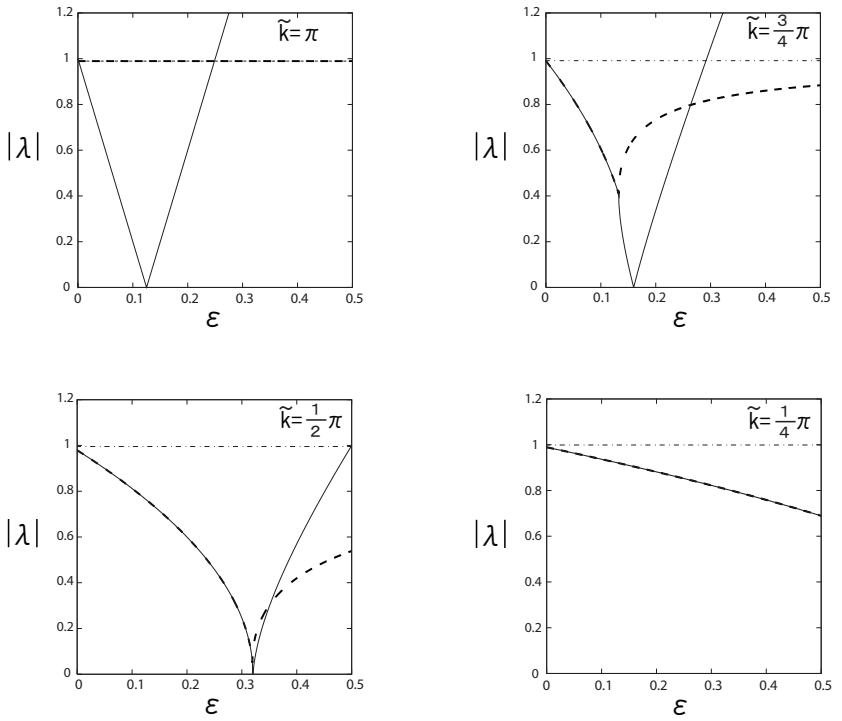

Figure 2: The magnitudes of the eigenvalues for ACM-Bulk versus ϵ; $\nu = 0.001$, $\beta = 2$, $\mu = 1$, $\tau = 1$, and $\chi = (1/s_2 - 1/2)/3$ ($s_2 = 1.63$). The solid line, the dashed line, and the dash dotted line indicate $|\lambda_a|$, $|\lambda_b|$, and $|\lambda_c|$, respectively.

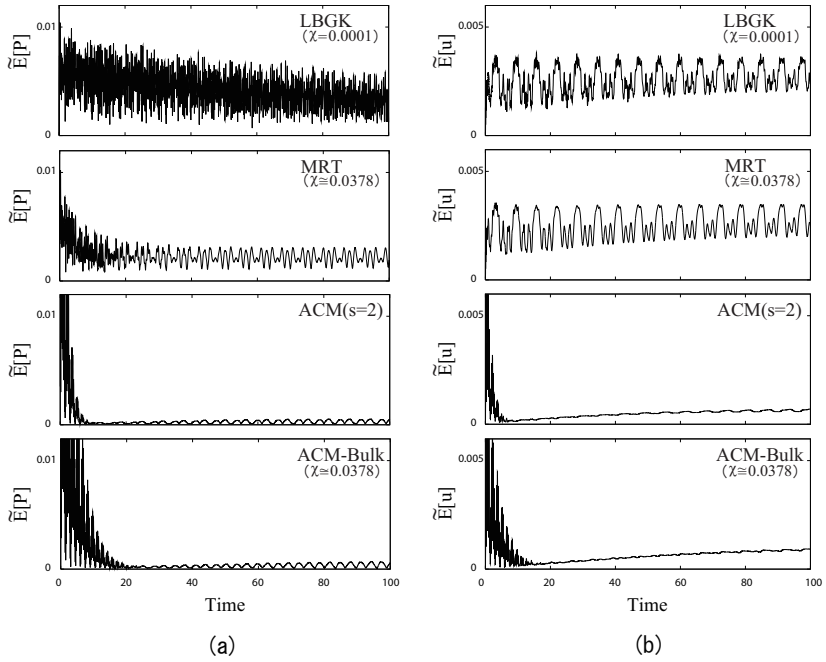

Figure 3: The time history of L^1 errors $\tilde{E}[h]$ $(h = u, P)$ in the generalized Taylor-Green problem $(\nu, k, U, \theta, \epsilon) = (0.001, 1, 1, \pi/12, \pi/32)$.

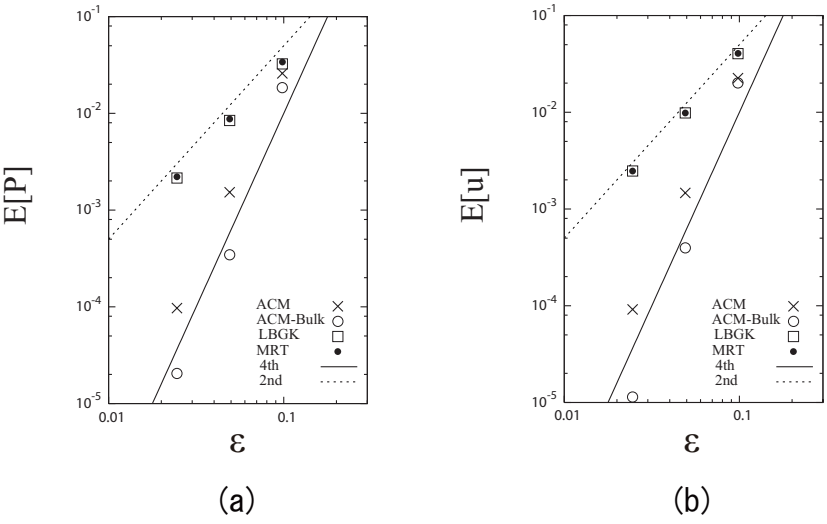

Figure 4: The L^∞ error $E[h]$ $(h = u, P)$ versus ϵ at $t = 100$ in the generalized Taylor-Green problem for $(\nu, k, U, \theta) = (0.001, 4, 1, \pi/12)$. The results of the fortified ACM $(s = 2)$, ACM-Bulk $[\chi \sim 0.0378$ $(s_2 = 1.63)]$, LBGK $(\chi = 0.001)$, and MRT-LBM $[\chi \sim 0.0378$ $(s_2 = 1.63)]$ are plotted in the figure.

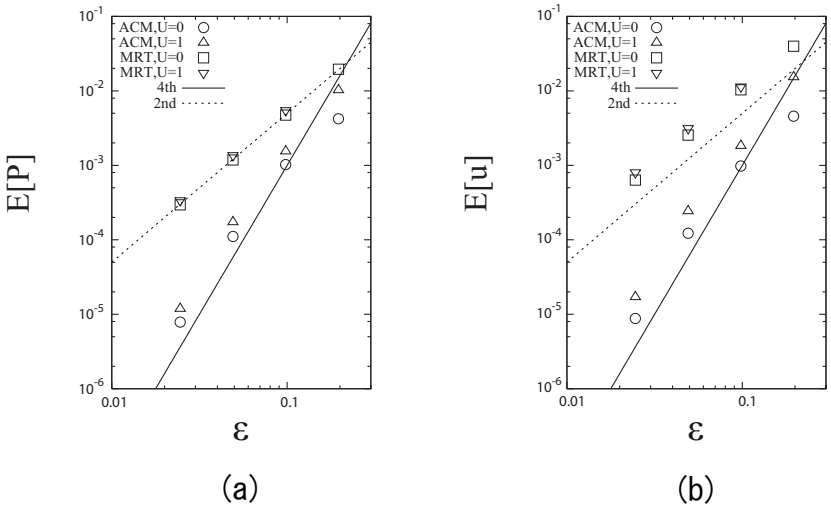

Figure 5: The L^∞ error $E[h]$ $(h = u, P)$ versus ϵ at $t = 100$ in the generalized Taylor-Green problem for $(\nu, k, \theta) = (0.001, 1, \pi/12)$ and $U = 0, 1$. The results of the fortified ACM $(s = 2)$ and MRT-LBM $(s_2 = 1.63)$ are plotted in the figure.

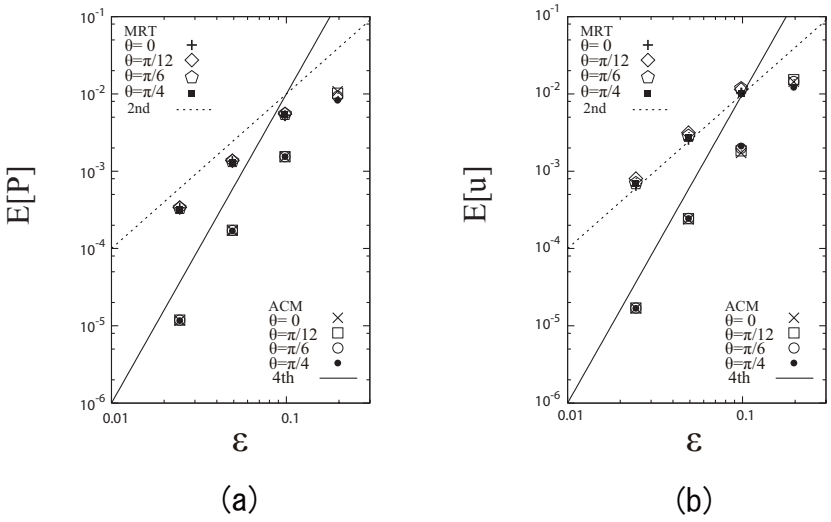

Figure 6: The L^∞ error $E[h]$ $(h = u, P)$ versus ϵ at $t = 100$ in the generalized Taylor-Green problem for $(\nu, k, U) = (0.001, 1, 1)$ and $\theta = 0, \pi/12, \pi/6, \pi/4$. The results of the fortified ACM $(s = 2)$ and MRT-LBM $(s_2 = 1.63)$ are plotted in the figure. The results of MRT-LBM are missing for the largest mesh spacing $\epsilon = \pi/16$ because of the breakdown of the computation.

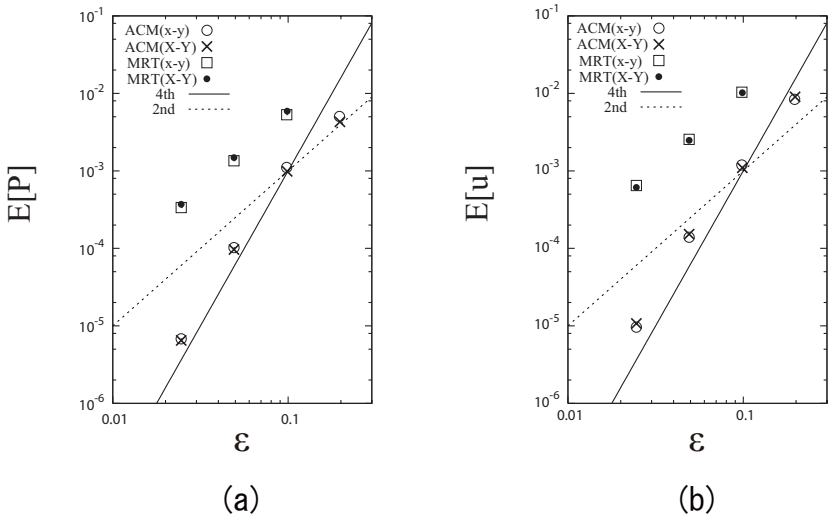

Figure 7: The L^∞ error $E[h]$ $(h = u, P)$ versus ϵ at $t = 100$ in the generalized Taylor-Green problem for $(\nu, k, U, \theta) = (0.001, 1, 1, 0)$. The results of ACM $(s = 2)$ and MRT-LBM $(s_2 = 1.63)$ are plotted in the figure. The symbols $\circ$ and $\square$, respectively, indicate the results of the fortified ACM $(s = 2)$ and MRT-LBM $(s_2 = 1.63)$ for xy coordinate system. The symbol $\times$ and $\bullet$, respectively, indicate the results of the fortified ACM $(s = 2)$ and MRT-LBM $(s_2 = 1.63)$ for XY coordinate system. The results of MRT-LBM are missing for the largest mesh spacing $\epsilon = \pi/16$ because of the breakdown of the computation.

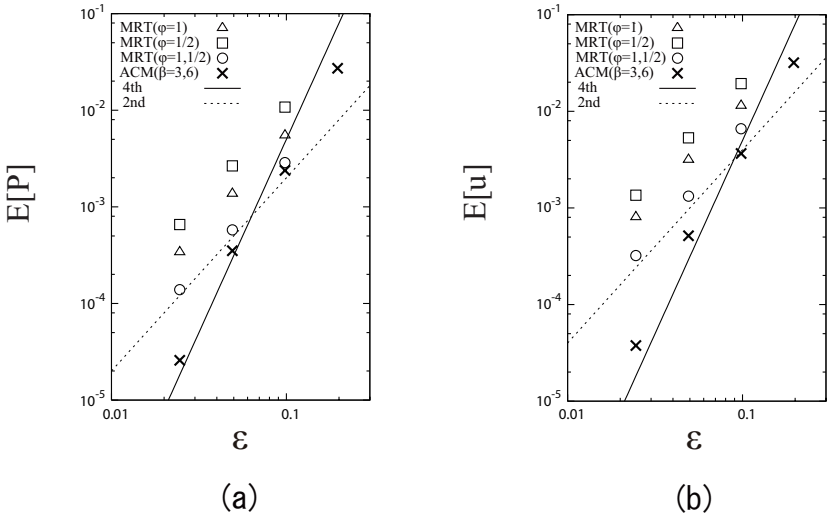

Figure 8: The L^∞ error $E[h]$ $(h = u, P)$ versus ϵ at $t = 100$ in the generalized Taylor-Green problem for $(\nu, k, U, \theta) = (0.001, 1, 1, 0)$. The results of the fortified ACM $(s = 2)$ and MRT-LBM with tunable Mach number $(s_2 = 1.63)$ are plotted in the figure. The symbols $\triangle$ and $\square$ indicate the results of MRT-LBM for $\varphi = 1$ and $\varphi = 1/2$, respectively. The symbol $\circ$ indicates the result obtained by the Richardson extrapolation from the MRT-LBM results for $\varphi = 1, 2$. The symbol $\times$ indicates the result obtained by the Richardson extrapolation from the results of the fortified ACM $(s = 2)$ for $\beta = 3, 6$. The results of MRT-LBM are missing for the largest mesh spacing $\epsilon = \pi/16$ because of the breakdown of the computation.